Wideband Bandpass-to-All-stop Reconfigurable Filtering Power Divider with Bandwidth Control and All-passband Isolation

Zheng Zhuang[1], Yongle Wu[1*], Yuanan Liu[1], and Zabih Ghassemlooy[2]

[1]School of Electronic Engineering, Beijing University of Posts and Telecommunications, P.O. Box. 282, 100876, Beijing, China
[2]Faculty of Engineering and Environment, Northumbria University, Newcastle upon Tyne, NE1 8ST, U.K.
*wuyongle138@gmail.com

Abstract: A novel wideband bandpass-to-all-stop reconfigurable filtering power divider is proposed in this paper, which allows for four-order bandpass-to-all-stop reconfigurable operating function and equal power division. Its circuit configuration includes the cascaded coupled-line sections with tight coupling to extend the impedance transforming. Furthermore, with the introduction of the half-wavelength open-circuit stubs, which controls the bandwidth, extra transmission poles located at the cut-off frequency are generated, thus resulting in high frequency selectivity. Moreover, by using a single resistor between input coupled-lines, the high all-passband isolation can be achieved. The grounding are then loaded to the output coupled-lines to enable bandpass-to-all-stop operating functionality. For demonstration, a prototype operating at 2 GHz is designed, simulated, and measured with a 15-dB bandwidth of 51%, 19-dB stopband rejection up to 5 GHz, and 14.5-dB all-passband isolation, which shows a good agreement between the simulated and measured results.

1. Introduction

Power dividers (PDs) are widely applied in microwave and wireless communication systems, especially in the power amplifiers, mixers, and antenna arrays. For further rejection of the interference signals at the radio frequency (RF)/microwave front end, filters connected in series with PDs are normally used, which results in a bulky circuit size and a high insertion loss. With the ever increasing demands for high performance microwave devices, PDs with filtering responses have been investigated extensively [1]-[18], owing to the high frequency selectivity and miniaturization.

In [1], two Butterworth filter transformers were integrated in Wilkinson PDs, leading to the two functions of the power split and filtering response. However, the narrow stopband feature limits its applications in multi-standard wireless communications. In order to extend the stopband suppressing the out-of-band interference, a compact net-type resonator was utilized to achieve the filtering power divider (FPD) with Chebyshev- or quasi-elliptic responses [2]. In addition, the two short-circuit half-wavelength stepped-impedance resonators [3] and dual mode resonators [4] were embedded into the conventional quarter-wavelength transmission lines (TLs), respectively, for the desired wide stopband. Nevertheless, the main shortcomings of these designed PDs with wide stopband are the very narrow passband and poor isolation. Hence, a simple stub-loaded ring resonator was presented to realize the wideband filtering response [5], but with no consideration of output isolation. For achieving high output isolation, the coupled-line section with a half-wavelength open-circuit stub was selected as a wideband bandpass FPD with high frequency selectivity in [6], [7] and further improvement in stopband rejection would be better. Moreover, the highly symmetric structure can also provide the improved in-band isolation, suffering from difficult accuracy fabrication [8]. Based on the coupled-line structure, a wideband filtering PD with

ultra-wide stopband is reported in [9], but the achieved high isolation needs lumped elements. In addition, researches working on FPDs have mostly focused on the arbitrary power ratios [10], [11], dual-band [12], [13] and multi-way operation [14], [15].

Besides, utilizing the integrated design of FPDs for miniaturization in multifunctional components, the tunable components can be used instead in multi-frequency systems [16]-[20]. In [16], the varactors loaded onto the open-end of each coupled-resonator were adopted to obtain the desired tunable frequency, which is difficult for maintaining the constant absolute bandwidth. By using varactors in place of the capacitors, which controls the coupling coefficients and external quality factors, frequency agility with a constant absolute bandwidth was realized [17], however the isolation should be further improved. Recently, combinations of inductor, capacitor, and varactors were adopted to design a frequency and bandwidth both controllable FPD [18]. The quasi-bandpass structure is used to achieve a reconfigurable single-/multi-band filtering power divider [19]. Based on the connection of resonators to the branches through impedance inverters, a Wilkinson-type power divider with tunable frequency and bandwidth is presented in [20]. In these reported investigations, the tunable devices generally used varactors or switches to tune the operating frequency or the bandwidth. To the best of authors' knowledge, there are few works reported on PDs with reconfigurable operating function applied in complex multifunctional systems.

In this paper, a wideband four-order bandpass-to-all-stop reconfigurable equal FPD is proposed based on the cascaded coupled-lines (CLs) with tight coupling and the centre loaded half-wavelength open-circuit stubs (OCSs). At first, two cascaded CLs are used for inherent impedance transformation with a filtering response for different terminated impedances. Then, by using the half-wavelength OCS, extra transmission poles (TPs) and zeros (TZs) are generated to ensure a wide stopband and a sharp cut-off in the four-order passband. Moreover, the passband bandwidth

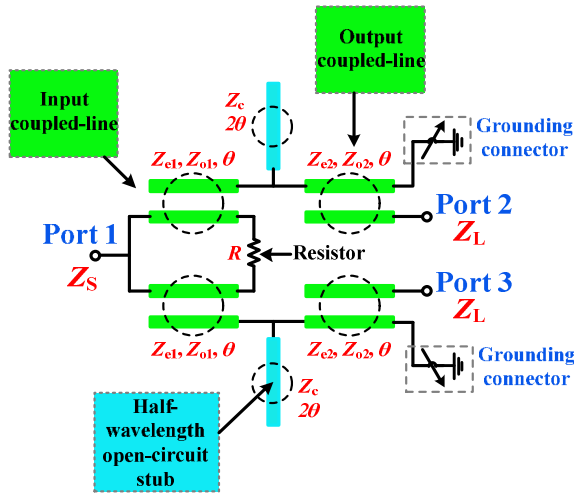**Fig. 1.** *The circuit configuration of the proposed bandpass-to-all-stop reconfigurable filtering power divider.*
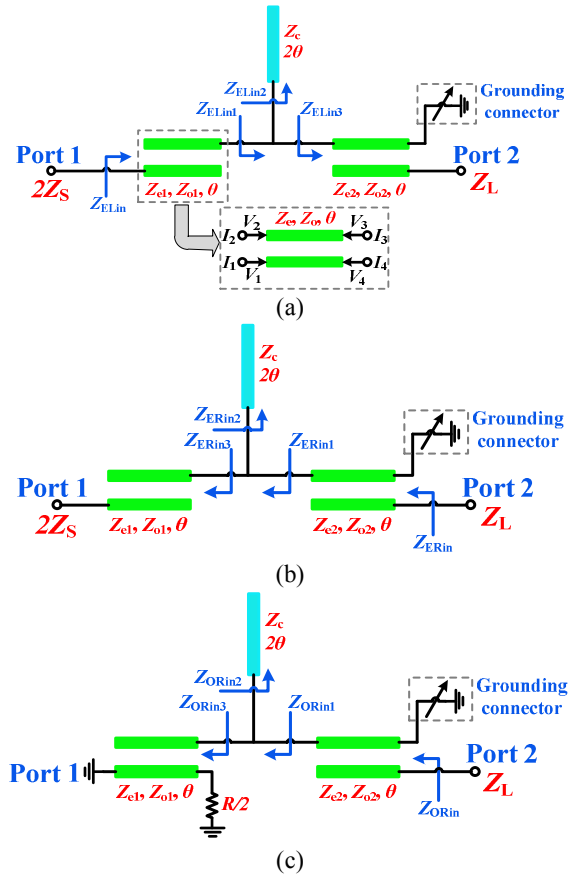

Fig. 2. *The equivalent circuits of the proposed wideband reconfigurable FPD: (a) even mode with left-hand side excitation, (b) even mode with right-hand side excitation, and (c) odd mode with right-hand side excitation.*

can be controlled effectively by the characteristic impedance of OCS. Finally, based on the even-/odd- mode analysis, good all-passband isolation is achieved using a single resistor. Additionally, all-stop operation is realized by grounding the open-end of output CL. To sum up, the main advantages of the proposed FPD can be summarized as: 1) good in-band return loss, 2) wideband bandwidth control, 3) high all-passband isolation, 4) bandpass-to-all-stop reconfigurable functionality, 5) arbitrary real terminated impedances, and 6) high stopband rejection and frequency selectivity with four TPs.

2. Design Theory of The Proposed FPD

Fig. 1 depicts the proposed wideband reconfigurable FPD circuit configuration, which is composed of cascaded CLs with tight coupling and centre-loaded half-wavelength OCSs. Based on even-/odd-mode analysis, the *S*-parameters of the designed FPD with arbitrary source and load impedances (Z_S, Z_L) can be obtained. Moreover, the corresponding even-/odd-mode equivalent circuits are illustrated as Fig. 2. For analysing the cascaded CLs, the generalized four-port CL structure with current and voltage definitions is depicted in Fig. 2(a) and the circuit models of the modified two-port CLs with different terminations are displayed in Fig. 3.

2.1. Even-mode analysis

In an even-mode equivalent circuit, the terminal currents of the modified two-port CL structure with open-circuit termination shown in Fig. 3(a) can be expressed as:

$$I_2 = I_4 = 0 \text{ or } I_1 = I_3 = 0. \tag{1}$$

Combining (1) with the TL theory [21], the impedance matrix of the two-port CL structure is deduced as:

$$[Z]_{CL1} = \begin{bmatrix} -jZ_a \cot\theta & -jZ_b \csc\theta \\ -jZ_b \csc\theta & -jZ_a \cot\theta \end{bmatrix}_{CL1}, \tag{2a}$$

where θ is the electrical length of CLs and for simplification we have assumed that

$$\begin{cases} Z_a = \dfrac{Z_e + Z_o}{2} \\ Z_b = \dfrac{Z_e - Z_o}{2} \end{cases}, \tag{2b}$$

where Z_e and Z_o are the even-/odd-mode impedances of the modified two-port CL structure, respectively. Then, based on (2) the even-mode input impedances of the wideband bandpass FPD with the left-hand side excitation as in Fig. 2(a) can be obtained:

$$\begin{cases} Z_{ELin3} = -jZ_{a2} \cot\theta + \dfrac{Z_{b2}^2 \csc^2\theta}{Z_L - jZ_{a2}\cot\theta} \\ Z_{ELin2} = -jZ_c \cot(2\theta) \\ Z_{ELin1} = \dfrac{Z_{ELin2} Z_{ELin3}}{Z_{ELin2} + Z_{ELin3}} \\ Z_{ELin} = -jZ_{a1}\cot\theta + \dfrac{Z_{b1}^2 \csc^2\theta}{Z_{ELin1} - jZ_{a1}\cot\theta} \end{cases}, \tag{3}$$

where Z_{a1}, Z_{a2}, Z_{b1}, and Z_{b2} can be calculated by (2b). Additionally, Z_c stands for the characteristic impedance of the half-wavelength OCS and Z_L denotes the load impedance.

Therefore, the reflection coefficient Γ_{in}^e at the input port 1 for the even-mode equivalent circuit and the corresponding parameter S_{11} of the proposed wideband bandpass FPD can be calculated as:

$$S_{11} = \Gamma_{in}^e = \dfrac{Z_{ELin} - 2Z_S}{Z_{ELin} + 2Z_S}. \tag{4}$$
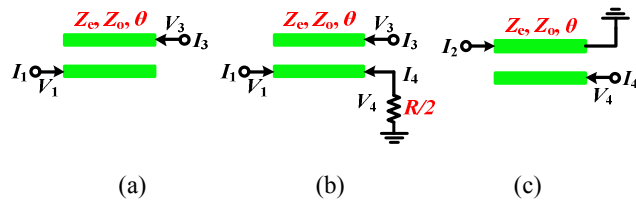
2

(a)　　　　　　　(b)　　　　　　　(c)

Fig. 3. *The circuit model of the modified two-port coupled-line with (a) two open-circuit terminations, (b) a single resistor (R/2), and (c) a short- and an open-circuit termination.*

where Z_S is the source impedance. Similarly, the even-mode input impedances of the wideband bandpass FPD with the right-hand side excitation as in Fig. 2(b) can be defined as:

$$\begin{cases} Z_{ERin3} = -jZ_{a1}\cot\theta + \dfrac{Z_{b1}^2\csc^2\theta}{2Z_S - jZ_{a1}\cot\theta} \\[2mm] Z_{ERin2} = -jZ_c\cot(2\theta) \\[2mm] Z_{ERin1} = \dfrac{Z_{ERin2}Z_{ERin3}}{Z_{ERin2} + Z_{ERin3}} \\[2mm] Z_{ERin} = -jZ_{a2}\cot\theta + \dfrac{Z_{b2}^2\csc^2\theta}{Z_{ERin1} - jZ_{a2}\cot\theta} \end{cases} \quad (5)$$

Based on (5), the corresponding reflection coefficient $\Gamma_{out}^{\ e}$ at the output port 2 for the even-mode equivalent circuit is calculated as:

$$\Gamma_{out}^{\ e} = \frac{Z_{ERin} - Z_L}{Z_{ERin} + Z_L}. \quad (6)$$

2.2. Odd-mode analysis

In the odd-mode equivalent circuit, the terminal voltages and currents of the modified two-port CL structure with a single resistor ($R/2$) termination shown in Fig. 3(b) can be expressed as:

$$I_2 = 0,\ I_4 = -\frac{V_4}{R/2}. \quad (7)$$

Combining (7) with the TL theory [21], the impedance matrix of the two-port CL structure is deduced as:

$$[Z]_{CL2} = \begin{bmatrix} \dfrac{-Z_a^2\sin\theta + jZ_aR\cos\theta}{jZ_a\cos\theta - R\sin\theta} & \dfrac{jZ_bR}{jZ_a\cos\theta - R\sin\theta} \\[3mm] \dfrac{jZ_bR}{jZ_a\cos\theta - R\sin\theta} & \dfrac{(j(Z_a^2 - Z_b^2)\cos\theta - Z_aR\sin\theta)\cot\theta}{jZ_a\cos\theta - R\sin\theta} \end{bmatrix}_{CL2}. \quad (8)$$

and

$$\begin{cases} Z_a = \dfrac{Z_e + Z_o}{2} \\[2mm] Z_b = \dfrac{Z_e - Z_o}{2} \end{cases}. \quad (9)$$

Accordingly, based on (8) the odd-mode input impedances of the wideband bandpass FPD with the right-hand side excitation in Fig. 2(c) are given:

$$\begin{cases} Z_{ORin3} = \dfrac{jRZ_{a1}\cos\theta - Z_{a1}^2\sin\theta + \dfrac{R^2Z_{b2}^2\tan\theta}{j(Z_{a1}^2 - Z_{b1}^2)\cos\theta - RZ_{a1}\sin\theta}}{jZ_{a1}\cos\theta - R\sin\theta} \\[3mm] Z_{ORin2} = -jZ_c\cot(2\theta) \\[2mm] Z_{ORin1} = \dfrac{Z_{ORin2}Z_{ORin3}}{Z_{ORin2} + Z_{ORin3}} \\[2mm] Z_{ORin} = -jZ_{a2}\cot\theta + \dfrac{Z_{b2}^2\csc^2\theta}{Z_{ORin1} - jZ_{a2}\cot\theta} \end{cases} \quad (10)$$
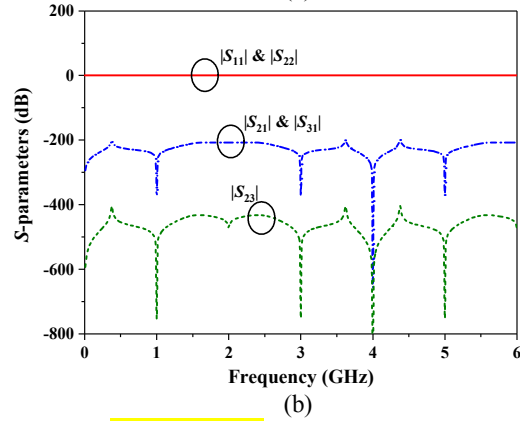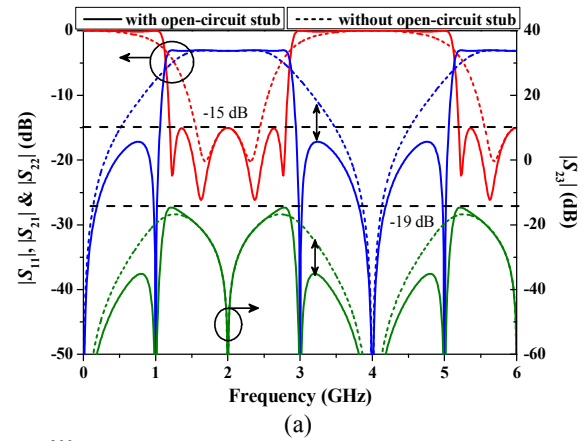

(a)

(b)

Fig. 4. *The ideal simulated S-parameters of the proposed: (a) bandpass and (b) all-stop FPD.*

Based on (10), the corresponding reflection coefficient $\Gamma_{out}^{\ o}$ at the output port 2 for the odd-mode equivalent circuit is calculated as:

$$\Gamma_{out}^{\ o} = \frac{Z_{ORin} - Z_L}{Z_{ORin} + Z_L}. \quad (11)$$

In order to achieve the good all-passband isolation, the parameter S_{23} needs to be given:

$$S_{23} = \frac{\Gamma_{out}^{\ e} - \Gamma_{out}^{\ o}}{2}, \quad (12)$$

where $\Gamma_{out}^{\ e}$ and $\Gamma_{out}^{\ o}$ are the reflection coefficients at the output port for the even-/odd-mode equivalent circuit, respectively, which can be calculated by (6) and (11). According to the required input matching S_{11} with a wideband filtering response and high isolation condition ($S_{23}=0$), the corresponding characteristic impedances of CLs with the electrical length of 90° (i.e., $\theta=90°$ at the centre frequency) and half-wavelength OCSs can be obtained based on (4) and (12). Fig. 4 shows the S-parameters as a function of the frequency for the proposed FPD with optimal impedances of $Z_{e1}=153$ Ω, $Z_{o1}=14.4$ Ω, $Z_{e2}=168.6$ Ω, $Z_{o2}=51.4$ Ω, and with/without the OCS of $Z_c=105$ Ω. For the proposed bandpass FPD with OCSs, the bandwidth of 15-dB return loss is 80% across the 1.2-2.8 GHz frequency band. The all-passband isolation achieved by a single resistor of 140 Ω is below -19 dB. And the stopband suppression is better than 17 dB up to 5 GHz. However, for the bandpass FPD without OCSs, the in-band return loss is greater than 15 dB with a bandwidth of 44% over the frequency range of 1.56 to 2.44 GHz. And the stopband suppression and the
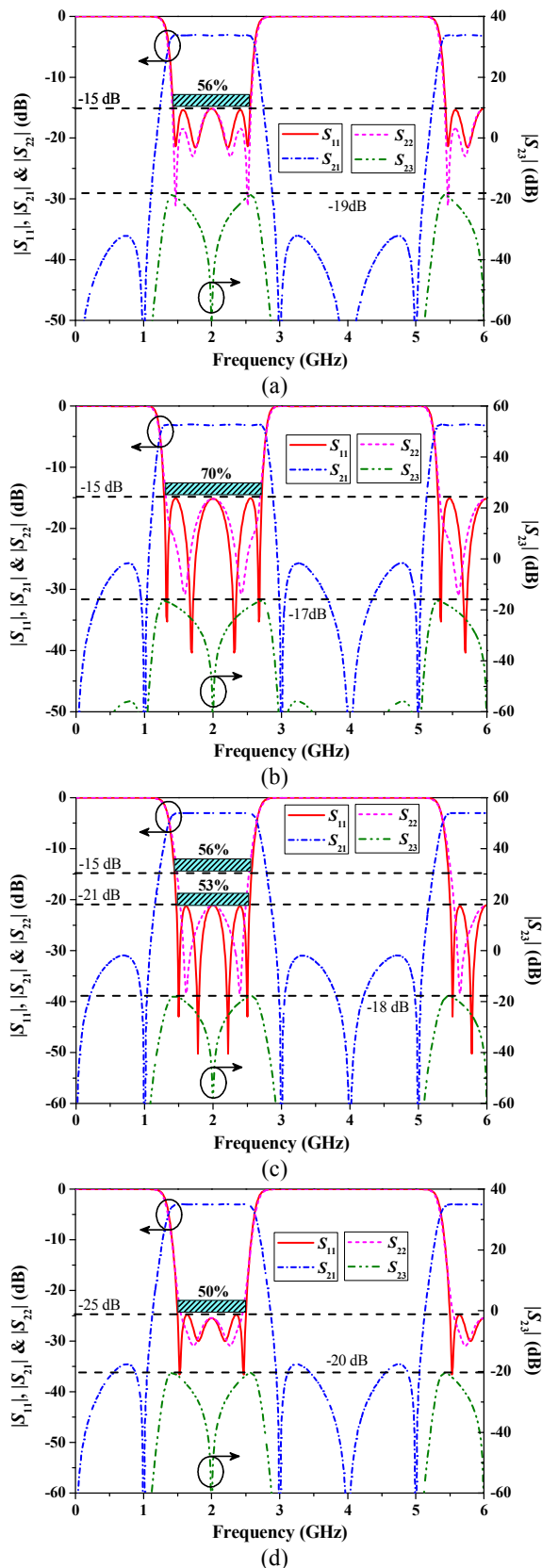
3

Fig. 5. *The ideal simulated S-parameters for typical four cases: (a) A, (b) B, (c) C, and (d) D.*

Table 1 Different parameters of The Four Cases

Case	Design Goal	Design Parameter
A	FBW: 56% RL (in-band):-15 dB Isolation:-19 dB $Z_S=Z_L=50$ Ω	$Z_{e1}=152.7$ Ω; $Z_{o1}=46$ Ω; $Z_{e2}=160$ Ω; $Z_{o2}=70$ Ω; $Z_c=28$ Ω; $R=197$ Ω; $\theta=0.5\pi$;
B	FBW: 70% RL (in-band):-15 dB Isolation:-17 dB $Z_S=Z_L=50$ Ω	$Z_{e1}=158$ Ω; $Z_{o1}=30$ Ω; $Z_{e2}=173$ Ω; $Z_{o2}=65$ Ω; $Z_c=60$ Ω; $R=177$ Ω; $\theta=0.5\pi$;
C	FBW: 56% (15 dB) RL (in-band):-21 dB Isolation:-18 dB $Z_S=Z_L=50$ Ω	$Z_{e1}=139$ Ω; $Z_{o1}=22$ Ω; $Z_{e2}=162.4$ Ω; $Z_{o2}=72$ Ω; $Z_c=31$ Ω; $R=130$ Ω; $\theta=0.5\pi$;
D	FBW: 50% RL (in-band):-25 dB Isolation:-20 dB $Z_S=40$; $Z_L=60$ Ω	$Z_{e1}=150$ Ω; $Z_{o1}=46$ Ω; $Z_{e2}=160$ Ω; $Z_{o2}=65$ Ω; $Z_c=28$ Ω; $R=240$ Ω; $\theta=0.5\pi$;

FBW: Fractional bandwidth; RL: Return loss

out-of-band isolation are attenuated by 6 dB and 10 dB, respectively. Therefore, from Fig. 4(a) it can be seen that the half-wavelength OCS can add extra TPs at the cut-off frequency for extending the bandwidth and improving the skirt selectivity with no additional insertion loss. Furthermore, the stopband suppression and out-of-band isolation are also improved. Note that the modified two-port CL with short- and open-ends, see Fig. 3(c), would become an all-stop filtering structure [22], thus leading to the potential of bandpass-to-all-stop transformation as depicted in Fig. 4(b). For all-stop case, the ideal insertion loss ($|S_{21}|$) and isolation ($|S_{23}|$) are larger than 200 dB and 400 dB, respectively.

3. Example analysis of the proposed FPD

For verify our proposed analytical design approaches and circuit structure, four typical numerical examples are designed and simulated. Fig. 5 illustrates the S-parameters with different properties, including fractional bandwidth, in-band return loss, isolation, and insertion loss. The corresponding circuit parameters are listed in Table 1. All examples are simulated by Advanced Design System (ADS) software.

In Fig. 5(a), the in-band return loss is better than 15 dB with a bandwidth of 56% ranged from 1.44 to 2.56 GHz. And the 19-dB isolation is across the entire passband. Additionally, the stopband suppression is below -36 dB up to 5 GHz. Next, in Fig. 5(b) maintaining the in-band return loss better than 15 dB, the bandwidth is added to 70% from 1.79 to 2.71 GHz by mainly increasing the value of the characteristic impedance for the half-wavelength OCS, whereas the in-band isolation and stopband suppression are declined to -17 dB and -25.7 dB, respectively. Compared Fig. 5(a) with Fig. 5(c), the in-band return loss can be improved to 21 dB with maintaining the 15-dB bandwidth of 56% by mainly changing the tight degree of the input CL while the in-band isolation and stopband suppression are reduced to -18 dB and -31 dB, respectively. Moreover, the bandwidth of 21-dB in-band return loss is about 53%, thus
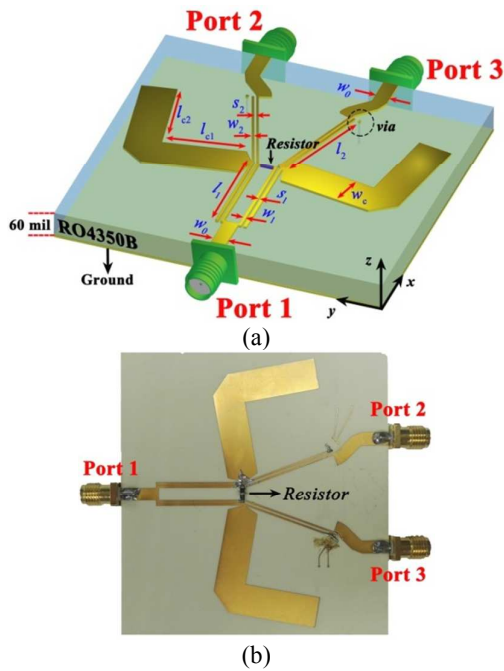
4

(a)

(b)

Fig. 6. *(a) Layout and (b) photograph of the proposed wideband reconfigurable FPD circuit.*

displaying high frequency selectivity. In addition, for the proposed FPD with different terminated impedances and with the in-band return loss greater than 25 dB, the wide passband is within frequency range of 1.5 to 2.5 GHz.

Accordingly, as shown in Fig. 5(a) and 5(b), although the stopband suppression is reduced with increasing the bandwidth, an excellent in-band return loss (S_{11}) and a high all-passband isolation (S_{23}) can still be achieved. The bandwidth of the proposed wideband passband FPD can be mainly controlled by the half-wavelength OCS. Moreover, maintaining the bandwidth unchanged, the in-band return loss can be defined artificially by the tight degree of the input CL from Fig. 5(c), thus leading to improve flexibility in practical applications. In addition, even though the source and load impedances are different in Fig. 5(d), an improved performance can also be achieved by using the proposed design approach. Compared with other reported works [1]-[18], the proposed FPD in this paper can achieve an improved return loss of <-15 dB, a controllable wideband bandwidth of >50%, all-passband isolation of <-15 dB, higher stopband suppression of <-15 dB, and a reconfigurable circuit structure (bandpass-to-all-stop).

4. Implementation and measured results

In order to verify the developed theoretical concept, we have selected one of cases in Section III i.e., the Case A operating at the center frequency f_0 of 2 GHz in Fig. 5 for fabrication on a RO4350B substrate with a relative permittivity of 3.48, loss tangent of 0.0037, and thickness of 1.524 mm. Fig. 6 shows the layout and photograph of the designed wideband reconfigurable FPD showing the main dimensions: w_1=0.72 mm, s_1=0.1 mm, l_1=23.47 mm, w_2=0.56 mm, s_2=0.43 mm, l_2=24.45 mm, w_c=8 mm, l_{c1}=18.75 mm, l_{c2}=19.9 mm, and w_0=3.43 mm. The size of the circuit configuration is $0.88\lambda_g \times 0.88\lambda_g$. Note that the via hole is used to achieve bandpass-to-all-stop transformation
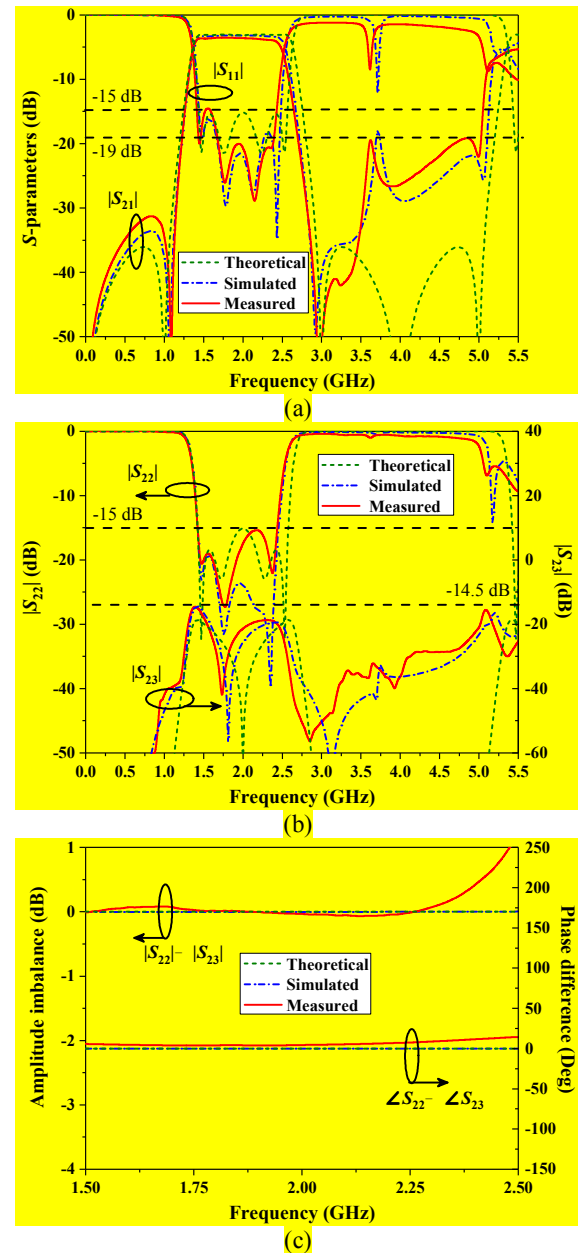

(a)

(b)

(c)

Fig. 7. *The theoretical, EM simulated and measured results of the proposed bandpass FPD: (a) S_{11} and S_{21}, (b) S_{22} and S_{23}, and (c) phase imbalance and amplitude imbalance.*

by means of grounding. The electromagnetic (EM) simulations are performed by Advanced Design System (ADS) software, and the measured results are obtained by the vector network analyzer of ROHDE&SCHWARZ ZVA8.

Fig. 7 and Fig. 8 illustrate the theoretical, EM simulated and measured results. As shown in Fig. 7(a), for the 15-dB in-band return loss the measured bandwidth is about 51% within the frequency range of 1.41-2.43 GHz, and the measured stopband suppression is better than 19 dB up to 5 GHz. Furthermore, from Fig. 7(b) the measured isolation is below -14.5 dB across the entire passband, and the maximal measured isolation is 42.1 dB near the operating band. Additionally, the measured $|S_{21}|$ and $|S_{31}|$ parameters at 2 GHz are about 3.62 dB and 3.59 dB,
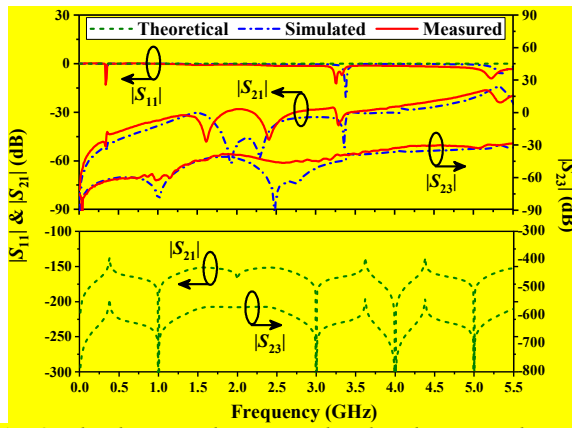
5

Fig. 8. The theoretical, EM simulated and measured results of the proposed all-stop FPD.

respectively, whereas the in-band phase different in Fig. 7(c) between the two output ports is about 4.4°. By grounding the output CL section, the theoretical, EM simulated, and measured results for the all-stop FPD are shown in Fig. 8. For all-stop case, the measured insertion loss ($|S_{21}|$) and isolation ($|S_{23}|$) are higher than 14 dB and 25 dB, respectively. It can be seen that there is a good agreement between the simulated and measured results, thus validating the proposed circuit configuration and design theory. In fact, the phase constant of coupled line under even- and odd-mode excitation are not exactly the same in theory, especially for high frequency case. However, this difference can be generally ignored in circuit analysis. Therefore, the discrepancies between theoretical and measured results are created in practical applications, but the good performances including return loss, isolation, and stopband suppression still can be obtained, as shown in Fig. 7. Besides, the discrepancies in Fig. 8 may be produced by the fabricated via holes simulating ground, connector losses, the effect of soldering, and manufacturing errors. Finally, a comparison between the proposed FPD and other published works is listed in Table 2.

To the best authors' knowledge, this work is the first to report on achieving a wideband bandpass-to-all-stop reconfigurable filtering power divider. In comparison with the other work in this field, see Table 2, the proposed equal FPD has a wide bandwidth and an excellent return loss. Though the bandwidth reported in [5] and [6] are higher, the proposed FPD scheme, as in Case B and shown in Fig. 5(b), achieves similar performance due to inherent bandwidth controllability. Moreover, the all-passband isolation is below -14.5 dB, which is better than that in [2]-[5], comparable with that in [6]. Although the isolation achieved in [17] and [18] is higher, their stopband suppression was not considered. Additionally, by locating the extra TPs at the cut-off frequency in the proposed scheme, the skirt selectivity has been enhanced.

5. Conclusion

In this paper, a novel wideband reconfigurable filtering power divider with bandpass-to-all-stop responses and equal power division, as well as a controllable bandwidth feature is proposed. The analysis and circuit configuration is also provided, followed by the verification of a design example with a 15-dB bandwidth of 51%, 19-dB

Table 2 Comparison with Other Reported Works

Refs.	f_0 (GHz)	FBW/RL (Inband)	BW/IL (Stopband)	Isolation	BC[1]/ BPTAS[2]
[2]	0.9	4.2% 19 dB	$5f_0$ 28 dB	11 dB All-passband	–/–
[3]	0.9	22.2% 10 dB	$22.2f_0$ 10 dB	20 dB Narrow band	–/–
[4]	2.41	4.1% 10 dB	$1.8f_0$ 15 dB	10 dB Narrow band	–/–
[5]	2.05	62% 10 dB	$0.95f_0$ 16 dB	10 dB Narrow band	–/–
[6]	3.01	70% 14 dB	f_0 13 dB	15 dB All-passband	+/–
[17]	0.62–0.85	4.4%–6% 10 dB	–	16 dB All-passband	–/–
[18]	1.3–2.08	4.8%-7.7% 10 dB	–	26 dB All-passband	+/–
This work	2	51% 15 dB	$1.2f_0$ 19 dB	14.5 dB All-passband	+/+

RL: Return loss; IL: Insertion loss
[1]Bandwidth control
[2]Bandpass-to-all-stop

stopband suppression, and 14.5-dB isolation across the entire band by means of simulation and experiment. The proposed circuit with a wideband controllable bandwidth, good all-passband isolation, bandpass-to-all-stop reconfigurable function, impedance transforming, and high stopband rejection and frequency selectivity, is attractive in modern wireless communication systems.

6. Acknowledgments

7. References

[1] Deng, P.-H. and Chen, Y.-T.: 'New Wilkinson power dividers and their integration applications to four-way and filtering dividers', IEEE Trans. Compon. Packag. Manufact. Technol., 2014, 4, (11), pp. 1828–1837

[2] Chen, C.-F., Huang, T.-Y., Shen, T.-M., and Wu, R.-B.: 'Design of miniaturized filtering power dividers for system-in-a-package', IEEE Trans.Compon. Packag. Manufact. Technol., 2013, 3, (10), pp. 1663–1672

[3] Chau, W.-M., Hsu, K.-W., and Tu, W.-H.: 'Wide-stopband Wilkinson power divider with bandpass response', Electron. Lett., 2014, 50, (1), pp. 39-40

6

[4] Song, K.: 'Compact filtering power divider with high frequency selectivity and wide stopband using embedded dual-mode resonator', Electron. Lett., 2015, 51, (6), pp. 495-497

[5] Gao, S. S., Sun, S., and Xiao, S. Q.: 'A novel wideband bandpass power divider with harmonic-suppressed ring resonator', IEEE Microw.Wireless Compon. Lett., 2013, 23, (3), pp. 119–121

[6] Zhang, B. and Liu, Y. A.: 'Wideband filtering power divider with high selectivity', Electron. Lett., 2015, 51, (23), pp. 1950-1952

[7] Kim, P., Jeong, J., Chaudhary, G., and Jeong, Y.: 'A design of unequal termination impedance power divider with filtering and out-of-band suppression characteristics', in Proc. Microwave Conference (EUMC), Sep. 2015, pp. 123-126

[8] Chen, C.-F. and Lin, C.-Y.: 'Compact microstrip filtering power dividers with good in-band isolation performance', IEEE Microw. Wireless Compon. Lett., 2014, 24, (1), pp. 17–19

[9] Wu, Y., Zhuang, Z., Liu, Y., Deng, L., and Ghassemlooy, Z.: 'Wideband filtering power divider with ultra-wideband harmonic suppression and isolation', IEEE Access, 2016, 4, pp. 6876-6882

[10] Wu, Y., Zhuang, Z., Yan, G., Liu, Y., and Ghassemlooy, Z.: 'Generalized dual-band unequal filtering power divider with independently controllable bandwidth', IEEE Trans. Microw. Theory Techn., 2017, 65, (10), pp. 3838-3848

[11] Wang, K., Zhang, X., and Hu, B.-J.: 'Gysel power divider with arbitrary power ratios and filtering responses using coupling structure', IEEE Trans. Microw. Theory Techn., 2014, 62, (3), pp. 431–440

[12] Li, Y. C., Xue, Q., and Zhang, X. Y.: 'Single- and dual-band power dividers integrated with bandpass filters', IEEE Trans. Microw. Theory Techn., 2013, 61, (1), vol. pp. 69-76

[13] Li, Q., Zhang, Y., and Fan, Y.: 'Dual-band in-phase filtering power dividers integrated with stub-loaded resonators', IET Microw. Antennas Propag., 2015, 9, (7), pp. 695-699

[14] Chen, F.-J., Wu, L.-S., Qiu, L.-F., and Mao, J.-F.: 'A four-way microstrip filtering power divider with frequency-dependent couplings', IEEE Trans. Microw. Theory Techn., 2015, 63, (10), pp. 3494–3504

[15] Zhu, H., Abbosh, A. M., and Guo, L.: 'Wideband four-way filtering power divider with sharp selectivity and wide stopband using looped coupled-line structures', IEEE Microw. Wireless Compon. Lett., 2016, 26, (6), pp. 413–415

[16] Chen, C.-F., Lin, C.-Y., Tseng, B.-H., and Chang, S.-F.: 'Compact microstrip electronically tunable power divider with Chebyshev bandpass response', in Proc. Asia Pacific Microw. Conf., Nov. 2014, pp. 1291–1293.

[17] Gao, L., Zhang, X., and Xue, Q.: 'Compact tunable filtering power divider with constant absolute bandwidth', IEEE Trans. Microw. Theory Techn., 2015, 63, (10), pp. 3505–3513

[18] Chi, P.-L. and Yang, T.: 'A 1.3–2.08 GHz filtering power divider with bandwidth control and high in-band isolation', IEEE Microw. Wireless Compon. Lett., 2016, 26, (6), pp. 407–409

[19] Psychogiou, D., Gomez-Garcia, R., Guyette, A. C., and Peroulis, D.: 'Reconfigurable single-/multi-band filtering power divider based on quasi-bandpass sections', IEEE Microw. Wireless Compon. Lett., 2016, 26, (3), pp. 684–68

[20] Gomez-Garcia, R., Psychogiou, D., and Peroulis, D.: 'Fully-tunable filtering power dividers exploiting dynamic transmission-zero allocation', IET Microw. Antennas Propag., 2017, 11, (3), pp. 3078–3085

[21] Pozar, D. M.: 'Microwave Engineering, Third ed.', New York, NY, USA: Wiley, 2005.

[22] Jones, E. M. T. and Bolljahn, J. T.: 'Coupled-strip-transmission-line filters and directional couplers', IRE Trans. Microw. Theory Techn., 1956, 4, (2), pp. 75–81

7